Encapsulation of Silicon Nanoclusters in Zeolite Y†

Jiliang He, Yong Ba, Christopher I. Ratcliffe,* John A. Ripmeester, Dennis D. Klug, John S. Tse, and Keith F. Preston

Contribution from the Steacie Institute for Molecular Sciences, National Research Council of Canada, 100 Sussex Drive, Ottawa, Ontario, Canada K1A 0R6

Received May 8, 1998

Abstract: Luminescent silicon clusters have been synthesized by the chemical vapor deposition of Si_2H_6 into the α-cages of $H_{32}Na_{24}Y$ zeolite. The synthetic process was monitored by FTIR, TGA-MS, and ^{29}Si and ^1H solid-state NMR spectroscopies. In the initial step at 100 °C, Si_2H_6 reacts with the Brønsted acid sites to produce anchored $ZO-Si_2H_5$. Si_2H_6 is also chemisorbed at Na^+ cation sites to give Si_2H_6/NaHY and is possibly physically trapped within the α-cage by the anchored disilyl groups. Multiple quantum ^1H NMR spin counting shows that each α-cage contains 38 H atoms. This is equivalent to 14 Si atoms present as a combination of disilyl and disilane. Subsequent thermal treatment of the entrapped disilane precursors leads, via H_2 and SiH_4 elimination, to the formation of Si clusters. The formation of Si clusters is complete at 550 °C. These clusters are capped by up to 5 H atoms (determined by ^1H NMR spin counting) and attached to the zeolite framework through SiO_x linkages (determined by Si K-edge XANES). The average size of the resulting silicon clusters is 12 ± 2 Si atoms (determined by XPS and Si K-edge XANES). The encapsulated Si clusters are air-stable and exhibit a room-temperature photoluminescence in the green-yellow region with a peak energy at ∼2.2 eV. The HOMO−LUMO energy gap in the Si cluster is estimated to be 2.2 eV, from a comparison of the band edges of the Si clusters and bulk Si (c-Si) (determined by synchrotron photoabsorption (Si K-edge XANES) and photoemission spectroscopies). The close correspondence of the HOMO−LUMO energy gap and the photoluminescence peak energy confirms the origin of luminescence from the Si cluster as a predominantly electron−hole radiative recombination process.

Introduction

The encapsulation of semiconductor nanoclusters in the pores of zeolite molecular sieves has been actively explored as a means of producing tunable light-emitting materials.[1−3] The well-defined and well-organized cavities provided by a zeolite host serve as an ideal nanoreactor for the synthesis of semiconductor clusters of controlled size and shape, in an ordered array. This approach also has the advantage of stabilizing the possibly very unstable nanosized clusters through encapsulation and coordination to the host framework. While encapsulated II−IV semiconductor clusters in zeolites have been extensively studied,[4−8] relatively little work has been systematically carried out on III−V[9] and IV[10,11] clusters, particularly Si clusters, in such systems.

The intense current interest in luminescent silicon clusters and nanocrystals is motivated by the suggestion that quantum confinement effects are responsible for the strong room-temperature photoluminescence from porous Si (por-Si)[12] and the potential applications of these luminescent Si materials in Si-compatible optoelectronic devices.[13] Several chemical approaches have been used to prepare Si clusters and nanocrystals, including solution-phase synthesis via the dehalogenation of halosilanes by alkali metals[14] or KSi,[15] ultrasonic fracturing of porous Si,[16] and gas-phase depositions by either slow combustion[17] or microwave plasma[18] of silanes. Generally a wide size

* Corresponding author: (tel) 613-991-1240; (fax) 613-998-7833; (e-mail) cir@ned1.sims.nrc.ca.

† Published as NRCC No. 40887.

(1) (a) Stucky, G. D.; MacDougall, J. E. *Science* **1990**, *247*, 669. (b) Srdanov, V. I.; Blake, N. P.; Markgraber, D.; Metiu, H.; Stucky, G. D. In *Advanced Zeolite Science and Applications*; Jansen, J. C., Stocker, M., Karge, H. G., Weitkamp, J., Eds.; Studies in Surface Science and Catalysis 85; Elsevier Science: New York, 1994; p 115.

(2) Herron, N. *J. Inclusion Phenom. Mol. Recognit. Chem.* **1995**, *21*, 283.

(3) Ozin, G. A. In *Materials Chemistry: An Emerging Discipline*; Interrante, L. V., Casper, L. A., Ellis, A. B., Eds.; Advances in Chemistry Series 245; American Chemical Society: Washington, DC, 1995; Chapter 14.

(4) Herron, N.; Wang, Y.; Eddy, M. M.; Stucky, G. D.; Cox, D. E.; Moller, K.; Bein, T. *J. Am. Chem. Soc.* **1989**, *111*, 530.

(5) Wang, Y.; Herron, N. *J. Phys. Chem.* **1988**, *92*, 4988.

(6) Liu, X.; J. K. Thomas, J. K. *Langmuir* **1989**, *5*, 58.

(7) Jentys, A.; Grimes, R. W.; Gale, J. D.; Catlow, C. R. A. *J. Phys. Chem.* **1993**, *97*, 13535.

(8) (a) Steele, M. R.; Macdonald, P. M.; Ozin, G. A. *J. Am. Chem. Soc.* **1993**, *115*, 7285. (b) Ozin, G. A.; Steele, M. R.; Holmes, A. J. *Chem. Mater.* **1994**, *6*, 999.

(9) MacDougall, J. E.; Eckert, H.; Stucky, G. D.; Herron, N.; Wang, Y.; Moller, K.; Bein, T.; Cox, D. *J. Am. Chem. Soc.* **1989**, *111*, 8006.

(10) Dag, Ö.; Kuperman, A.; Ozin, G. A. *Adv. Mater.* **1994**, *6*, 147.

(11) (a) Ozin, G. A.; Dag, Ö.; Kuperman, A.; Macdonald, P. M. *Stud. Surf. Sci. Catal.* **1994**, *84*, 1107. (b) E. Chomski, E.; Dag, Ö.; Kuperman, A.; Coombs, N.; Ozin, G. A. *Chem. Vap. Deposition* **1996**, *2*, 8.

(12) (a) Canham, L. T. *Appl. Phys. Lett.* **1991**, *57*, 1046. (b) Lehmann, V.; Gosele, U. *Appl. Phys. Lett.* **1991**, *58*, 856.

(13) For reviews; see: (a) Brus, L. *J. Phys. Chem.* **1994**, *98*, 3575. (b) Dag, Ö.; Kuperman, A.; Ozin, G. A. *Adv. Mater.* **1995**, *7*, 72. (c) King, W. D.; Boxall, D. L.; Lukehart, C. M. *J. Cluster Sci.* **1997**, *8*, 267.

(14) (a) Heath, J. R. *Science* **1992**, *258*, 1131. (b) Sekiguchi, A.; Sakurai, H. *Adv. Organomet. Chem.* **1995**, *37*, 1.

(15) Bley, R. A.; Kauzlarich, S. M. *J. Am. Chem. Soc.* **1996**, *118*, 12461.

(16) (a) Heinrich, J. L.; Curtis, C. L.; Credo, G. M.; Kavanagh, K. L.; Sailor, M. J. *Science* **1992**, *255*, 66. (b) Bley, R. A.; Kauzlarich, S. M.; Davis, J. E.; Lee, H. W. H. *Chem. Mater.* **1996**, *8*, 1881.

(17) (a) Fojtik, A.; Weller, H.; Fiechter, S.; Henglein, A. *Chem. Phys. Lett.* **1987**, *134*, 477. (b) Littau, K. A.; Szajowski, P. F.; Muller, A. J.; Kortan, A. R.; Brus, L. E. *J. Phys. Chem.* **1993**, *97*, 1224. (c) Wilson, W. L.; Szajowski, P. J.; Brus, L. E. *Science* **1993**, *262*, 1242.

10.1021/ja9816133 CCC: $15.00 Published 1998 by the American Chemical Society
Published on Web 10/01/1998

distribution of Si nanoparticles is produced with these methods. A narrow size range may only be obtained with further chromatographic separation[17b,c] or recrystallization processes.[14b] To study the correlation of electronic structure and optical properties with the particle size or to understand quantum confinement effects, it is desirable to produce uniform, size-selected Si clusters or nanocrystals.

In the continuing search for monodispersed Si clusters, Ozin and co-workers[11a] have explored the synthesis of Si nanoclusters in dehydrated HY zeolite through the chemical vapor deposition (CVD) of Si_2H_6 gas. They reported that the encapsulated Si clusters exhibited blue-shifts of their optical absorption edge with respect to bulk Si and strong room-temperature photoluminescence. The exact nature of these Si clusters, however, remains elusive. Previously we reported preliminary XPS and XANES studies of (a) the thermolysis products of a fully acid HY zeolite initially loaded with only ~4 Si_2H_6/cage, for which a cluster size of about 2−5 Si/cage was estimated,[19a] and (b) the cluster size as a function of disilane loading in NaHY,[19b] which showed that above a certain saturated loading crystalline Si was deposited on the outside of the zeolite particles.

In the present work, we have investigated some key aspects associated with the intrazeolitic Si clusters, which were synthesized in the α-cages of $H_{32}Na_{24}Y$ by the chemical vapor deposition of Si_2H_6 at the saturation loading determined earlier. Our objectives were to gain a better understanding of the encapsulation process, to determine the cluster size by spectroscopic methods, and to elucidate the electronic structure and luminescent properties. To this end, we have applied in situ FTIR, solid-state NMR, and TG-MS to monitor the formation of Si clusters, the multiple quantum ^{1}H NMR spin-counting technique to quantitatively analyze the number of disilane precursors entrapped in the α-cage of zeolite Y and the number of protons remaining in the Si clusters, XPS and Si K-edge XANES to determine the size of the cluster,[19] synchrotron photoabsorption and photoemission spectroscopies to study the HOMO−LUMO energy gap, and photoluminescence spectroscopy to study the optical behavior of the Si cluster. A coherent picture of the encapsulation process and the size of the Si clusters has emerged. This work has also established a clear correlation between the electronic structure and the luminescent properties.

Experimental Section

Sodium Y zeolite (LZ-Y52) with the unit cell composition $Na_{56}(AlO_2)_{56}(SiO_2)_{136}{\cdot}xH_2O$ was supplied by Union Carbide. Various acid forms of the zeolite $H_nNa_{56-n}Y$ ($n = 0$, 32, 51, determined by elemental analysis by Galbraith Labs. Inc.) were prepared from the sodium zeolite by exchanging the Na^+ cations with NH_4^+ cations followed by thermal dehydration and deammination. A typical ion exchange consisted of stirring 5 g of zeolite with 100 mL of 1.0 N NH_4NO_3 solution at 80 °C for 1−4 h. Thermal dehydration−deammination of the exchanged $(NH_4)_nNa_{56-n}Y$ zeolite was carried out by heating the material from 25 to 430 °C at 1 °C/min and then holding the temperature at 430 °C for 2 h under 10^{-3} Torr vacuum. This treatment produces an acidic form of zeolite denoted as $H_nNa_{56-n}Y$ with $n = 32$, 51. We specifically chose the partially exchanged $H_{32}Na_{24}Y$ form since it has better thermal stability than the highly acidic forms of Y zeolite.

Silicon clusters were prepared by the CVD of disilane gas (98%, Matheson) within the pores of the NaHY zeolites. The disilane gas was transferred into a closed vessel containing the dehydrated−deamminated zeolite powder through a vacuum line equipped with a pressure gauge. The mixture was then heated at 100 °C for 40 h. This treatment produced intrazeolitic disilane precursors. The loading of Si_2H_6 was roughly estimated according to the quantity of zeolite used and the amount of Si_2H_6 reacted. After removal of the H_2 evolved and unreacted Si_2H_6 by pumping at 100 °C for 1 h, the precursor was further heated to 550 °C at 1 °C/min and held at this temperature for 2 h. The resulting solid is stable in air and is pale yellow to brown, depending on the initial disilane loading. Samples were stored in a drybox before further characterization. Analysis of all these zeolitic Si cluster materials, with the exception of $H_{51}Na_5Y$, by powder XRD reveals that the crystallinity and integrity of the zeolite Y host is maintained and there are no diffraction peaks characteristic of crystalline silicon (c-Si). $H_{51}Na_5Y$ loses its framework crystallinity but appears to retain a periodic pore structure, as witnessed by a single sharp line at low angle in the XRD.

IR spectra were recorded on a Bio-Rad FTS-40A spectrometer equipped with a N_2 purge assembly and a liquid N_2-cooled mercury−cadmium−telluride detector (at resolution of 4 cm^{-1}). The $(NH_4)_nNa_{56-n}$-Y zeolite was pressed into a thin wafer which was placed in a reaction cell consisting of a fused-silica tube and a NaCl (4000−600 cm^{-1}) window. This cell allows the in situ IR spectroscopic observation of the thermal dehydration−deammination of the exchanged zeolite, the anchoring of Si_2H_6, and the clustering reaction of the intrazeolitic disilane precursor into Si clusters. After the thermal dehydration−deammination treatment, the zeolite wafer was exposed to 80 Torr of Si_2H_6 in the closed cell at 100 °C for 40 h. After the removal of the generated H_2 and unreacted Si_2H_6, the wafer was heated to 550 °C at 1 °C/min and held at this temperature for 2 h. Prior to the IR measurement, the sample was always degassed at 100 °C for 30 min.

^{29}Si CP MAS NMR experiments were carried out at 59.63 MHz on a Bruker AMX-300 spectrometer equipped with a double-resonance MAS probe. ^{29}Si chemical shifts were measured relative to $(CH_3)_4Si$ (TMS). Samples were packed in zirconia rotors and sealed with airtight O-ring caps under an inert atmosphere. The MAS frequencies in these experiments were ~6.2 kHz. The CP contact time was 5 ms. The scans ranged from hundreds to thousands, depending on the proton content of the sample. Two-dimensional multiple-quantum ^{1}H NMR spin-counting experiments were performed with a high-power static sample probe, following in essence the work of Pines et al.[20] The pulse sequence involves the following: (1) a preparation period consisting of a sequence of eight $p = \pi/2$ pulses, four with $+x$ phase, and then four with $-x$, with intervals of $2\Delta + p$ and Δ alternately between the pulses, repeated m times; (2) a mixing period again consisting of repeated eight pulse cycles, but with four $+y$ and four $-y$ $\pi/2$ pulses; and (3) a detection period which is followed by a $\pi/2$ reading pulse. A stepwise phase increment was used in the preparation period for modulating the magnetization belonging to different multiple-quantum coherence orders at the end of the mixing period. Only one cycle of phase incrementation (from 0 to 360°) was necessary in this experiment. Different multiple quantum excitation times were obtained by varying the number of cycles (m) of the eight pulse sequences, both in the preparation period and the mixing period. $p = 2$ μs and $\Delta = 4$ μs were used in these experiments.

Luminescence spectra were collected using an Ar^+ Coherent Innova 90 laser operated at a wavelength of 488 nm with the beam dispersed over a 1-mm^2 sample area (10 mW/cm^2). Samples were placed as wafers inside a cell (similar to the IR cell) with fused-silica windows that was evacuated to ~10^{-5} Torr. The emitted light was collected by a quartz lens and focused on the entrance slit of a Spex 1403 monochromator. Appropriate cutoff filters were used to remove scattered excitation radiation. The output of the monochromator was monitored by a Hamamatsu model R928 multialkali cooled side-on photomultiplier tube operated at 1700 V. The luminescence data were acquired by use of a Spectracq multichannel analyzer which was interfaced to an IBM personal computer with Spectramax software.

(18) Takagi, H.; Ogawa, H.; Yamazaki, Y.; Ishizaki, A.; Nakagiri, T. *Appl. Phys. Lett.* **1990**, *56*, 2379.

(19) (a) He, J.; Klug, D. D.; Tse, J. S.; Preston, K. *J. Chem. Soc., Chem. Commun*. **1997**, *1265*. (b) He, J.; Klug, D. D.; Tse, J. S.; Ratcliffe, C. I.; Preston, K. *Appl. Phys. Lett.* **1997**, *71*, 3194.

(20) (a) Munowitz, M.; Pines, A. *Science* **1986**, *233*, 525. (b) Baum, J.; Pines, A. *J. Am. Chem. Soc.* **1986**, *108*, 7447. (c) Munowitz, M.; Pines, A. *Adv. Chem. Phys.* **1987**, *66*, 1. (d) Lacelle, S. *Adv. Magn. Opt. Reson.* **1991**, *16*, 17. (e) Ba, Y.; Veeman, W. S. *Solid State Nucl. Magn. Reson.* **1993**, *2*, 131.

Si K-edge absorption spectra were measured at the double-crystal monochromator (DCM) beam line of the Canadian Synchrotron Radiation Facility (CSRF) at the Synchrotron Radiation Center, University of Wisconsin—Madison. Details of the DCM monochromator have been described elsewhere.[21] In essence, photons from the storage ring (1 GeV, ~100−150 mA) were monochromatized by reflection from two asymmetrically mounted InSb(111) crystals. Samples were mounted on indium foil (99.99% pure, Johnson Matthey) stacked on a stainless steel disk which was packed in an aluminum holder. They were then transferred to the ionization chamber. Data were obtained using the total electron yield (TEY). No charging was observed during the measurement. The resolution is ~0.06 eV for the absorption spectra.

The photoemission spectra were measured using the Grasshopper monochromator beam line at CSRF. A photon energy of 150 eV was used. All data were obtained with the TEY method. To reduce the charging problem, the sample was mixed with an electroconductive carbon powder in a weight ratio of 1:1 and then mounted on indium foil for measurement. The resolution is ~0.2 eV for the photoemission spectra at a photon energy of 150 eV.

XPS spectra were recorded on a Kratos Axis XPS instrument, using monochromated Al Kα radiation. Samples were mounted on an analysis stub with copper tape. The effective sampling depth is ~50 Å. A survey spectrum was run from 1000 to 0 eV to determine the elements present on the surface. High-resolution spectra were then run on the elements of interest or on all elements present for quantitative analysis.

Thermogravimetry (TG) and differential thermal analysis (DTA) of the intrazeolitic disilane precursor was performed on a DuPont TG/DTA instrument. Samples (~20 mg) were transferred in a platinum pan to the instrument under an inert atmosphere. Care was taken to avoid any contact of the sample with air. They were then heated at a rate of 5 °C/min from 50 to 600 °C. A flow of N_2 (~100 mL/min) was maintained during the TGA runs.

The evolution of volatile products during the clustering reaction of the intrazeolitic precursor leading to the formation of Si clusters was monitored with a quadrupole mass spectrometer (UTI 100C Precision Mass Analyzer) using an ionization energy of 75 eV. Samples (~10 mg) were placed in a quartz tube which was connected to the UHV chamber for mass detection. The quartz tube was heated at a rate of 5 °C/min from 100 to 500 °C. A scan from 1 to 150 amu was collected every minute throughout the thermal process. This technique permits the identification of the different gases evolved during thermolysis. The evolution of the ionic currents of the characteristic ions were plotted as a function of temperature. In the absence of standardization, only qualitative information may be drawn from these curves.

Results and Discussion

Encapsulation Process. This work in effect combines the host−guest inclusion chemistry based on zeolite Y with the method of chemical vapor deposition for the synthesis of zeolite-entrapped Si clusters. The encapsulation of Si_2H_6 within the pores of zeolite Y, its anchoring by reaction with −OH sites and Si clustering via thermolysis was monitored by in-situ IR, TGA-MS, and solid-state ^{29}Si MAS NMR spectroscopy.

(a) Anchoring of Si_2H_6. Figure 1 shows the evolution of the infrared spectra for the chemical vapor deposition of disilane, leading to the formation of silicon clusters. Prior to the addition of Si_2H_6, the ammonium-exchanged zeolite Y was dehydrated−deamminated at 430 °C under vacuum. The IR spectrum (Figure 1a) reveals diagnostic $\nu_{OH\alpha}$ (3636 cm^{-1}) and $\nu_{OH\beta}$ (3546 cm^{-1}) stretching frequencies of the Brønsted acid sites in the α-cages and β-cages (also commonly described as the supercage and the β-cage)[22] respectively, in the as-prepared $H_{32}Na_{24}Y$ zeolite. At room temperature, Si_2H_6 molecules are simply adsorbed in the α-cage, without chemical reaction. However, reaction with the OH groups via the elimination of H_2 takes place readily at 100 °C. The IR spectra show a decreasing intensity of the ν_{OH} stretching bands (3636, 3546 cm^{-1}) of the Brønsted acid sites concomitant with an increase in the intensity of the ν_{SiH} stretching bands (2195, 2151 cm^{-1}) as more Si_2H_6 reacts (Figure 1b,c). The Si−H_3 stretching vibrations between 2136 and 2179 cm^{-1} have been observed in both gas phase[23] and crystalline disilane.[24] Si−H_3 stretching vibrations between 2130 and 2154 cm^{-1} have also been reported from MIR−FTIR studies of disilane adsorption on Si(111)7 × 7.[25] Replacing one hydrogen with a more electronegative element (E), the (E)-Si−H_2 stretching vibration is expected to shift toward a higher wavenumber. Therefore, the bands at 2151 and 2195 cm^{-1} are attributed to the Si−H stretching modes in (Si)SiH_3 and (O)-(Si)SiH_2 groups, respectively. This suggests the formation of an anchored ZO−Si_2H_5 precursor. The reactivity of the H−Si bond in Si_2H_6 is sufficiently high to allow reaction with both α-cage and β-cage Brønsted acid sites at 100 °C. We calculate from structural information[23a,26] that the van der Waals diameter of an isotropically rotating Si_2H_6 is 6.73 Å, or if only rotating about the Si−Si axis, the cylindrical diameter is 5.19 Å, whereas the diameters of the cage windows are 7.4 Å for the 12-ring of the α-cage, 2.47 Å for the 6-ring of the β-cage, and 1.04 Å for the 4-ring of the hexagonal prism. It is very clear from these numbers that the Si_2H_6 must be restricted to the α-cage. The disappearance of the $\nu_{OH\beta}$ (3546 cm^{-1}) band therefore indicates that the protons in β-cages migrate to the α-cage where they react with Si_2H_6 at 100 °C. It has been reported that protons in zeolites are mobile at elevated temperature and can migrate even at room temperature if the adsorbates have sufficiently attractive powers (e.g., strong base).[27] IR spectroscopy indicates that excess Si_2H_6 is readily removed from the precursor following evacuation at 100 °C, after the initial reaction stage.

From the results of other experiments discussed below, we will show that the precursor has more disilanes per α-cage than

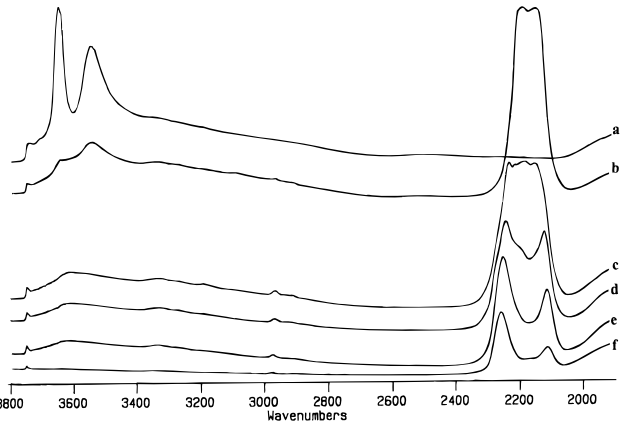

Figure 1. FTIR spectra of (a) $H_{32}Na_{24}Y$ host; (b) entrapped Si_2H_6 precursor/$H_{32}Na_{24}Y$ after 36 h at 100 °C; and after progressive heating for 1 h at (c) 250, (d) 350, (e) 450, and (f) 550 °C.

(21) Yang, B. X.; Middleton, F. H.; Olsson, B. G.; Bancroft, G. M.; Chen, J. M.; Sham, T. K.; Tan, K.; Wallace, D. J. *Nucl. Instrum. Methods* **1992**, *316*, 422.

(22) (a) Ward, J. W. *J. Catal.* **1967**, *9*, 225. (b) Uytterhoeven, J. B.; Jacobs, P.; Makay, K.; Schoonheydt, R. *J. Phys. Chem.* **1968**, *72*, 1768. (c) Ward, J. W.; Hansford, R. C. *J. Catal.* **1969**, *13*, 364.

(23) (a) Bethke, G. W.; Wilson, M. K. *J. Chem. Phys.* **1957**, *26*, 1107. (b) Nakamoto, K. *Infrared and Raman Spectra of Inorganic and Coordination Compounds*, 4th ed.; Wiley-Interscience Publ.: New York, 1986; p 164.

(24) Durig, J. R.; Church, J. S. *J. Chem. Phys.* **1980**, *73*, 4784.

(25) Uram, K. J.; Jansson, U. *Surf. Sci.* **1991**, *249*, 105.

(26) Eulenberger, G. R.; Shoemaker, D. P.; Keil, J. G. *J. Phys. Chem.* **1967**, *71*, 1812−1819.

(27) (a) Ward, J. W. *J. Phys. Chem.* **1969**, *73*, 2086. (b) Hughes, T. R.; White, H. M. *J. Phys. Chem.* **1967**, *71*, 2192.

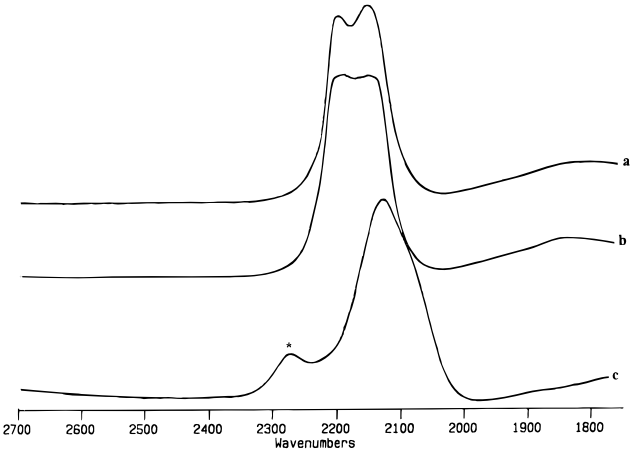

Figure 2. FTIR spectra showing νSiH stretching bands of anchored ZO−Si_2H_5 and chemisorbed Si_2H_6 in (a) $H_{51}Na_5Y$, (b) $H_{32}Na_{24}Y$, and (c) NaY. * indicates the line assigned to $(O)_3SiH$ due to the reaction of Si_2H_6 with defect sites.

can be attached at the four OH Brønsted acid sites per cage in $H_{32}Na_{24}Y$. It is possible that the extra molecules are simply trapped by the anchored molecules blocking the windows, but another strong possibility is that they are chemisorbed at Na^+ sites, if these are accessible (recall that some of the acid protons have migrated from the β-cages, so Na^+ may be needed there to effect charge balance with the framework). To identify the involvement of the Na^+ ion in the anchoring of Si_2H_6, several $H_nNa_{56-n}Y$ (n = 0, 32, 51) zeolite hosts were used for comparison. Figure 2 shows the ν_{Si-H} stretching bands of anchored ZO−Si_2H_5 and chemisorbed Si_2H_6NaY species in these hosts. The chemisorption of Si_2H_6 takes place inside the α-cage of $Na_{56}Y$ at room temperature, and these molecules cannot be pumped off. One single broad and asymmetric band was observed peaking at 2127 cm^{-1} for this chemisorbed species. When the temperature was increased to 100 °C, a weak band developed at 2274 cm^{-1}, while the major band at 2127 cm^{-1} remained the same. This weak band can be assigned to O_3SiH species, according to the literature.[28] (The formation of this band is probably due to the reaction of Si_2H_6 with some defect sites in the NaY zeolite.) The driving force for such chemisorption is most likely the polarization induced by the framework charge associated with the Na^+ cations and the pentacoordination of Si in the Si_2H_6 molecule with the framework oxygen. It is possible that both SiH_3 moieties are involved in the chemisorption, with two Na^+ sites, since only a single ν_{Si-H} stretching band was observed. The model of the chemisorbed state of Si_2H_6NaY is illustrated in Figure 3. The involvement of Na^+ cations in chemisorption inside the α-cage of Y zeolite has been observed for organometallic species (e.g., $Cd(CH_3)_2$, $Zn(CH_3)_2$, and $W(CO)_6$),[8,29] anhydrous hydrogen halides,[30] water,[31] and propyl halide.[32] Single or multication sites can be involved in the adsorption. The dipolar nature of the H−Si bond and the hypervalent coordinating nature of Si demand that one hydrogen atom will preferentially interact with the Na^+ cation, with the Si atom interacting with the framework oxygen. In $H_{32}Na_{24}Y$ zeolite, the Na^+ cations could also induce the chemisorption of Si_2H_6 at 100 °C, if they are accessible.

(28) Ling, L.; Kuwabara, S.; Abe, T.; Shimura, F. *J. Appl. Phys.* **1993**, *73*, 3018.
(29) Ozin, G. A.; Ozkar, S.; Macdonald, P. *J. Phys. Chem.* **1990**, *94*, 6939.
(30) Ozin, G. A.; Ozkar, S.; Stucky, G. D. *J. Phys. Chem.* **1990**, *94*, 7562.
(31) Ward, J. W. *Trans. Faraday Soc.* **1971**, *67*, 1489.
(32) Angell, C. L.; Howell, M. V. *J. Phys. Chem.* **1970**, *74*, 2737.

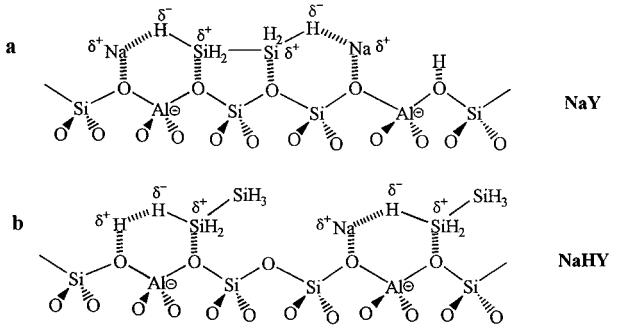

Figure 3. Schematic illustrations of the chemisorption of Si_2H_6 in (a) $H_{32}Na_{24}Y$ and (b) NaY.

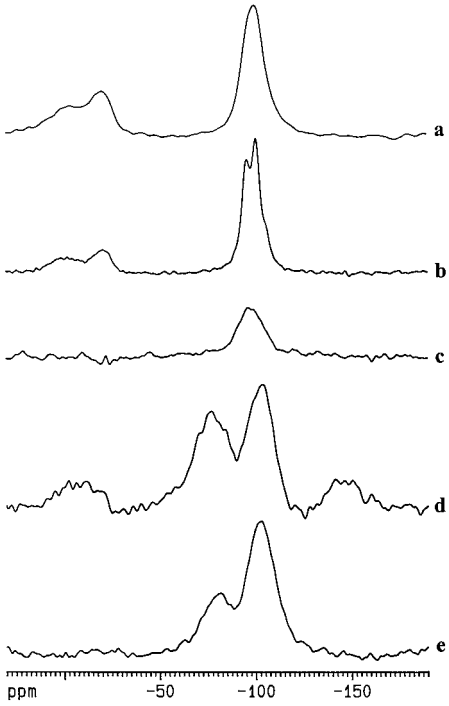

Figure 4. ^{29}Si CP MAS NMR spectra of the entrapped Si_2H_6 precursor in zeolite Y hosts, (a) $H_{51}Na_5Y$, (b) $H_{32}Na_{24}Y$, and (c) NaY, and the encapsulated Si clusters in (d) $H_{51}Na_5Y$ and (e) $H_{32}Na_{24}Y$. (Spinning side bands are apparent in (d) due to a slow spinning rate.)

Since the distribution of Na^+ sites in $H_{32}Na_{24}Y$ is rather different from $Na_{56}Y$ and the concentration of Na^+ cations in the α-cage is much lower than that in $Na_{56}Y$, the double-cation model shown in Figure 3a is not possible in this case. However, chemisorption at a single-cation site is feasible (Figure 3b). In this case, the ν_{Si-H} stretching band of the chemisorbed species is close to or overlapped with the anchored ZO−Si_2H_5. Therefore, at saturation the loading of Si_2H_6 consists of both framework-anchored ZO−Si_2H_5 and chemisorbed Si_2H_6NaHY. In $H_{51}Na_5Y$ zeolite, anchored ZO−Si_2H_5 is the predominant species.

The formation of anchored ZO−Si_2H_5 and chemisorbed Si_2H_6NaY were further confirmed by means of solid-state cross-polarization (CP) ^{29}Si MAS NMR. Figure 4a−c shows the ^{29}-Si CP-MAS NMR spectra of these entrapped disilane precursors in $H_{51}Na_5Y$, $H_{32}Na_{24}Y$, and $Na_{56}Y$, respectively. All the chemical shifts are referenced to tetramethylsilane (TMS).

Resonances from the silicons of the zeolite framework should occur in the −83 to −106 ppm region.[33] Unfortunately, the

(33) Engelhardt, G.; Michel, D. *High-Resolution Solid-State NMR of Silicates and Zeolites*; Wiley: New York, 1987; pp 228−229.

range of framework Si resonances overlaps the resonance of Si_2H_6 at −104.8 ppm and the range of resonances of $-SiH_3$ groups attached to another Si in polysilanes, i.e., −90 to −103 ppm.[34] All three disilane precursor materials display lines in these regions:[35] a broad featureless line centered at −100 ppm for $H_{51}Na_5Y$ (Figure 4a), sharper overlapping lines at −95 and −100 ppm and a shoulder at about −107 ppm for $H_{32}Na_{24}Y$ (Figure 4b), and a single broad resonance centered at −94 ppm for NaY (Figure 4c).

A cross-polarization signal for the NaY case confirms that disilane has been chemisorbed. Cross-polarization to the framework Si atoms in $Na_{56}Y$ has to occur from protons on the Si_2H_6 molecules and may be less efficient than in the HNaY cases, thus, we suspect, reducing the intensity of these signals.

With both $H_{51}Na_5Y$ and $H_{32}Na_{24}Y$ as host, two distinguishable broad resonances were observed centered at about −2 and −20 ppm (Figure 4a,b), which do not occur in the NaY case. The anchored $-O-Si_2H_5$ groups should have two quite distinct resonances; the $-SiH_3$ resonance we expect to remain in the −90 to −105 ppm region, whereas the $-O-SiH_2-$ resonance is expected to be shifted to significantly lower field. It is known that the ^{29}Si chemical shift is greatly deshielded when the Si atom is bonded to a more electronegative atom which has lone-pair p-hybridized orbitals for further conjugation, i.e., capable of σ- and π-bonding.[34b] For example, the ^{29}Si of SiH_4 resonates at −91.9 ppm, while SiH_3Cl is at −17.4 ppm; and the molecule $BrH_2Si^*Si^{**}H_3$ shows resonances at −42.3 ppm for Si* and −94.3 for Si**.[36] Furthermore, ab initio calculations (to be reported elsewhere) support this behavior. The fact that there are two low-field peaks, −2 and −20 ppm, most probably means that there are two distinct types of anchoring site on the cage framework. In the case of $H_{51}Na_5Y$ zeolite, the relative intensity of these two $ZO-SiH_2-$ silicon signals is proportionately larger than in $H_{32}Na_{24}Y$, which has fewer acid sites available for anchoring the disilane,

The chemical shifts for cation chemisorbed Si_2H_6 in $H_{32}Na_{24}Y$ (Figure 3b) are likely to be close to −94 ppm, the same as for Si_2H_6 in NaY and, unfortunately, once again overlapping with Si signals from the zeolite.

(b) Clustering Reaction. Upon thermal treatment, an intrazeolitic clustering reaction takes place progressively, leading to the formation of silicon clusters. This process is evident from the changes in the position and intensity of the ν_{SiH} stretching bands, as shown in Figure 1. At 250 °C, all residual hydroxyl groups have reacted with Si−H, since the intensities of ν_{OH} of ZOH_α and ZOH_β have decreased to zero. In addition to the decreasing ν_{SiH} stretching intensity, there clearly are a number of overlapping bands at about 2234, 2212, 2185, and 2148 cm^{-1}, which develop at this temperature. They are associated with O_2SiH_2, O_2SiSiH, $OSiSiH_2$, and $SiSiH_3$ species based on documented data.[11b,28,37] The intensity of the Si−H stretching bands decreased further with increasing temperature, and ultimately at 550 °C, the IR spectrum is dominated by two ν_{SiH} bands at 2258 and 2112 cm^{-1}, which are assignable to $(O)_3SiH$ (in framework defect sites) and OSi_2SiH (in Si clusters) species, respectively. This observation suggests that a dehydrogenation reaction occurs during heating and the Si clusters prepared at 550 °C are terminated with H and O.

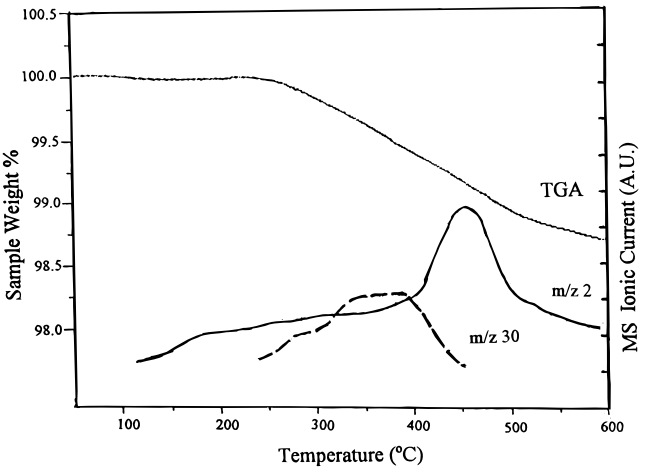

Figure 5. Thermogravimetric analysis (left-hand scale) and mass spectrometry (right-hand scale) for the entrapped Si_2H_6 precursor/$H_{32}Na_{24}Y$ as a function of temperature. The ion signal at *m*/*z* 2 (—) arises from H_2, and *m*/*z* 30 (- - -) from SiH_4.

Further insight into the clustering reaction was obtained by separate thermogravimetric analysis (TGA) and mass spectroscopy (MS) measurements on the entrapped disilane precursors, as shown in Figure 5. The precursors were prepared by the sorption of Si_2H_6 in $H_{32}Na_{24}Y$ at 100 °C, followed by vacuum removal of the physisorbed Si_2H_6. The measurements were then performed under a stringently dry, inert atmosphere (N_2) to avoid contact of the samples with moisture. The TGA curve shows mass loss from the precursor during heating from 50 to 600 °C, and MS qualitatively analyzes the gases evolved during this thermal process. The mass loss started at ∼270 °C and ended at ∼530 °C. A total mass loss of 1.5 wt % was observed and is accounted for by the evolution of SiH_4 and H_2, as detected in the MS. Hydrogen was detected at temperatures as low as 120 °C with maximum evolution at 460 °C, while SiH_4 started to evolve at ∼240 °C and finished at 430 °C, suggesting that both fragmentation and dehydrogenation reactions take place during this thermal process. No higher silane derivatives such as Si_2H_6 and Si_3H_8 were found by MS. SiH_4 was identified by the appearance of molecular fragments at *m*/*z* 30 (SiH_2^+, most abundant, shown in Figure 5), 31 (SiH_3^+), and 32 (SiH_4) in the MS spectra. It is interesting to note that hydrogen evolution is still detectable in the range of 550−600 °C, indicating that some hydrogen remains with the Si clusters, consistent with the IR result.

The formation of Si clusters from the sample prepared at 550 °C was examined by ^{29}Si CP MAS NMR spectroscopy. The result, shown in Figure 4d, shows two broad resonances which we assign in the same way as in previous work;[11a] the signal centered at −103 ppm is due to the zeolite framework Si, while the signal centered at −79 ppm must arise from the Si clusters. In a study of hydrogenated amorphous silicon, broad peaks were observed at about −63 ppm, which were shown, using cross-depolarization techniques, to envelop several components. One of these components in the region of −21 ppm was assigned to those Si nuclei which were hydrogenated.[38] We have observed the sharp resonance of c-Si at −81.3 ppm. The slight downfield shift of the −79 ppm peak from c-Si therefore probably reflects

(34) (a) Williams, E. A.; Cargioli, J. D. *Annu. Rep. NMR Spectrosc.* **1983**, *15*, 221. (b) Janes, N.; Oldfield, E. *J. Am. Chem. Soc.* **1985**, *107*, 6769.

(35) Preliminary results of ^{29}Si−^{27}Al double-resonance REAPDOR NMR experiments currently in progress[39] show that indeed there are some silicons in the same chemical shift region as the silicons of the zeolite framework, which have slightly longer distances to aluminum. This result supports the assignment of the chemical shift of the SiH_3 groups to the region −85 to −105 ppm.

(36) Hassler, K.; Koll, W.; Schenzel, K. *J. Mol. Struct.* **1995**, *348*, 353.

(37) (a) Tsue, D. V.; Lucovsky, G.; Davidson, B. N. *Phys. Rev. B* **1989**, *40*, 1795. (b) He, L.; Kurata, Y.; Inokuma, T.; Hasegawa, S. *Appl. Phys. Lett.* **1993**, *63*, 162.

(38) Zumbulyadis, N. *J. Chem. Phys.* **1987**, *86*, 1162.

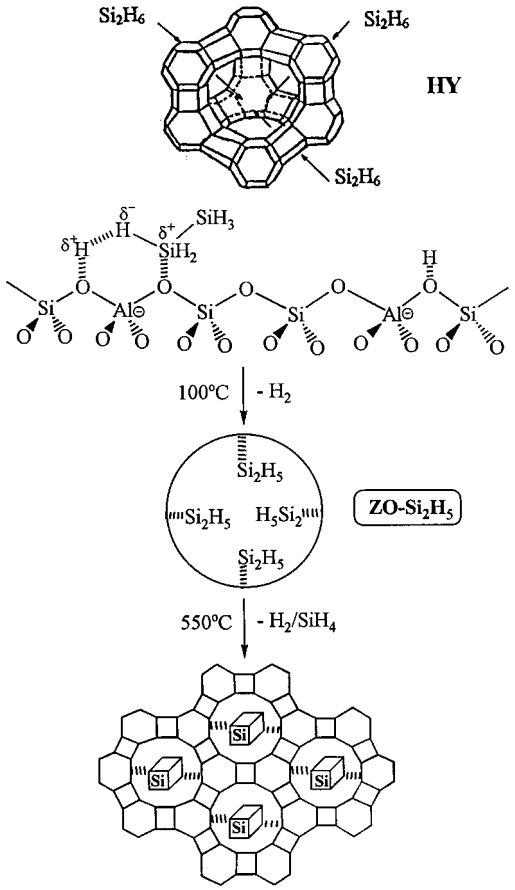

Figure 6. Schematic illustration of the encapsulation process of Si clusters in the α-cages of zeolite Y.

the partial hydrogenation of the cluster. The occurrence of intense spinning side bands associated with the −79 ppm signal indicates that the cluster silicons have a large chemical shift anisotropy. This suggests that the Si clusters are rigidly bound (to the framework oxygen) and that the Si sites are not symmetric (cf. the lack of spinning side bands for the framework Si atoms, which have a roughly tetrahedral environment). Bridging species SiO_x were observed by Si K-edge absorption spectroscopy (discussed below).

The stages in the formation of the encapsulated Si clusters can now be summarized as follows, (also shown schematically in Figure 6): Passing through the 7.5-Å diameter windows, Si_2H_6 molecules assemble inside the α-cages. Chemisorption of Si_2H_6 takes place at the cation and Brønsted acid sites. Anchored ZO−Si_2H_5 are generated via the dehydrocoupling reaction of an Si−H bond with an acid hydroxyl group at 100 °C. Upon further thermal treatment, these precursors undergo clustering reactions with the elimination of H_2 and SiH_4 to form Si clusters.

Size Determination. For the intrazeolitic semiconductor nanocluster systems, where the compositions of the constituent semiconductor cluster are different from those of zeolite (Al, Si, and O), chemical (or elemental) analysis is generally applied to quantify the size of the cluster in terms of the unit cell content of the zeolite. In the case of II−VI nanoclusters,[4,8,9] for example, it is also possible to measure the coordination shell of the cluster by using EXAFS technique. Therefore, the combination of chemical analysis and the EXAFS measurement has been employed to study the size and shape of such clusters. However, neither chemical analysis nor EXAFS is applicable to the intrazeolitic Si cluster system, since Si is present in both the cluster and the zeolite host. We therefore seek alternative techniques capable of spectroscopically discriminating the Si clusters from the zeolite host and thus quantitatively determining the size of Si clusters. In the first instance, we employed the 2D multiple-quantum ^{1}H NMR spin-counting technique to investigate the number of entrapped disilane precursors in the α-cage of zeolite Y. This gives a clue as to the maximum number of Si that can be obtained in the cluster. Since SiH_4 is evolved during the thermolysis, the size of the resulting Si cluster ought to be smaller than that measured from the entrapped disilane precursors, assuming that the silicons remain homogeneously distributed throughout the zeolite. Both XPS and Si K-edge XANES have also been applied to study the final cluster size.[19]

(a) Numbers of Entrapped Disilane Precursors/α-Cage: Multiple-Quantum ^{1}H NMR Spin Counting Study. ^{1}H spins in solids are connected via the internuclear dipole−dipole interaction to form an extended spin network. This network has multiple energy levels, with a broad range of magnetic quantum numbers, among which multiple-quantum (MQ) transitions can be excited. By subjecting the spin system to a period of MQ excitation, brought about by an rf multiple-pulse sequence, MQ coherences (which represent a collective behavior of the spins) can be generated.[20] Spins in close proximity, which have the strongest dipolar couplings, develop MQ coherence more rapidly than more distant ones. Therefore, with increasing excitation time, more spins become correlated to higher MQ coherence orders. For an infinite and homogeneously distributed spin system, MQ coherences grow continuously. However, for a finite coupled proton system, e.g., in the form of isolated clusters, the growth of coherence order levels off at a value corresponding to the number of protons in the cluster. Ultimately, at still longer times, clusters in relatively close proximity may also become correlated. Put another way, to assess the size of a cluster, the dipolar couplings between spins within the cluster must be large enough that MQ coherence with more distant spins cannot build up to any appreciable extent during the preparation period.

The generation and detection of the MQ coherence is carried out by means of a 2D NMR experiment. The MQ coherences are generated from the equilibrium state in the multipulse preparation period and then in the mixing period are refocused to the original state in order that a signal can be acquired. The signals in the 2D experiment are modulated by stepwise shifting of the radio frequency phase in the preparation period, so that the intensities of multiple-quantum coherence orders are obtained in the first dimension after Fourier transformation from the phase domain.

We have thus applied the MQ ^{1}H NMR technique to count the number of H atoms present in the entrapped disilane precursors in the α-cage of zeolite Y that are present as spatially isolated clusters. Shown in Figure 7 is the plot of the number of correlated spins as a function of excitation time for the sample of disilane entrapped in $Na_{24}H_{32}Y$. The correlated spin numbers were obtained by fitting the experimental intensities of the MQ coherence orders to a Gaussian distribution model. The number levels off at $N(\tau) = 38 \pm 1$ after 1500 μs. Since the $Na_{24}H_{32}Y$ host can only provide at maximum four ZOH groups per α-cage for anchoring ZO−Si_2H_5, i.e., 20 H/α-cage, the other 18 H's must come from three chemisorbed Si_2H_6NaHY. The error limit of ±1 also allows a combination of 3 ZO−Si_2H_5 and 4 Si_2H_6 for a total of 39 H. In either case, this accounts for a total of 7 disilane molecules entrapped in each α-cage and hence a maximum of 14 Si/α-cage. By use of the same technique, we also determined that a maximum of five residual protons are

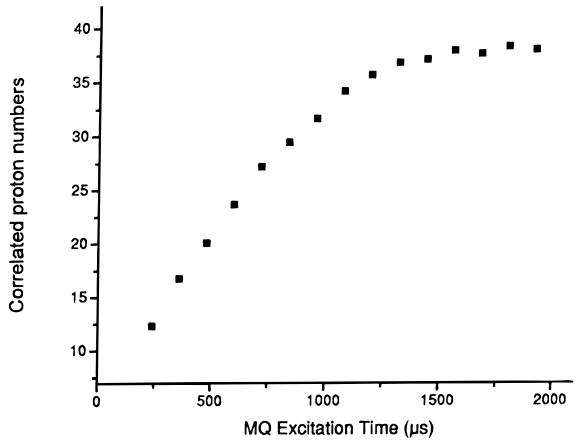

Figure 7. Number of correlated protons vs MQ excitation time for the entrapped Si_2H_6 precursor in $H_{32}Na_{24}Y$.

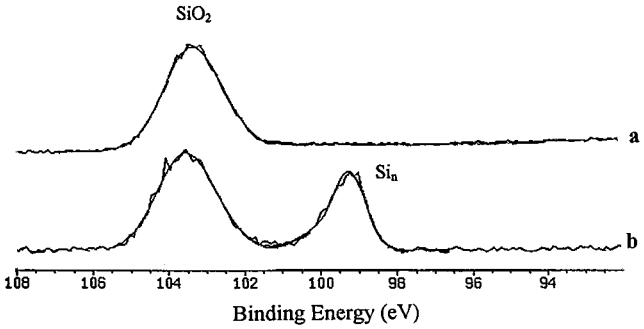

Figure 8. Si 2p XPS spectra of (a) $H_{32}Na_{24}Y$ and (b) the encapsulated Si clusters/ $H_{32}Na_{24}Y$.

associated with the Si clusters after thermolysis at 550 °C.[39] This work represents one of the few reported practical applications of MQ ^{1}H NMR spin counting and demonstrates the power of the technique for studying clusters in porous systems.

(b) Si Cluster Size: A Combination of XPS and XANES Studies. We have applied both X-ray absorption (Si K XANES) and photoelectron (XPS) spectroscopies to investigate the average size of the Si clusters. Both techniques provide electronic structural information about the intrazeolitic Si cluster nanocomposite, i.e., Si oxidation states. Thus, they avoid the inherent experimental difficulties of identifying and quantifying the Si clusters with the conventional elemental analysis technique. Figure 8 shows the Si 2p XPS spectra for the $H_{32}Na_{24}Y$ zeolite host and the intrazeolitic Si clusters. The peak at 99.3 eV, characteristic of the Si 2p binding energy for unoxidized Si, is attributed to Si clusters, while the peak at the binding energy of 103.9 eV corresponds to SiO_2 from the zeolite framework. Their relative concentrations are given by the ratio of the integral areas under the corresponding peaks. Based on the known number (136) of SiO_2 per unit cell of zeolite Y, the number of unoxidized Si atoms in the clusters per unit cell of zeolite Y is calculated to be 72 (≡9/cage).

The Si K XANES spectra for the intrazeolitic Si clusters, $H_{32}Na_{24}Y$ zeolite host, and c-Si are shown in Figure 9. The assignments of the edge absorptions were reported previously, i.e., 1840 eV for Si_n (unoxidized silicon in the clusters), 1845 eV for SiO_x (partly oxidized Si associated with the clusters), and 1847 eV for SiO_2 (Si of the zeolite framework).[19a] The relative concentrations of Si (clusters) and SiO_2 (framework of zeolite) in the composite are directly proportional to their respective edge jumps.[40] As commonly adopted,[41] the edge

(39) Ba, Y.; et al., to be published.

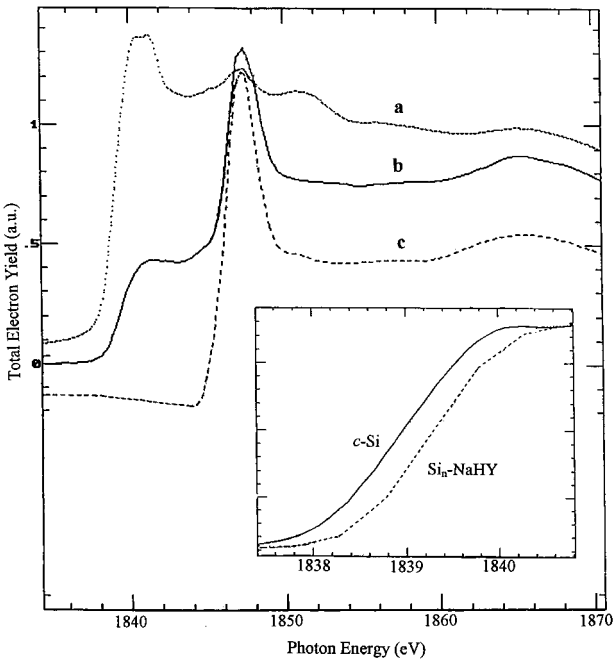

Figure 9. Si K-edge XANES data from (a) c-Si, (b) the encapsulated Si clusters/$H_{32}Na_{24}Y$, and (c) $H_{32}Na_{24}Y$. Inset shows the comparison of the Si absorption edges between c-Si and Si clusters.

jump is estimated by the difference of the signal in the flat region above the near-edge resonances and the signal just below the first resonance. From such a measurement, ~75 unoxidized Si atoms in the clusters per unit cell of zeolite Y are obtained. This result is in excellent agreement with that estimated by XPS. It is noteworthy that XPS is a surface-sensitive technique (effective sampling depth ~50 Å) whereas K-edge X-ray absorption measures both bulk and surface (sampling depth ~700 Å).[42] The similarity of the results from these two techniques further confirms that the Si clusters are homogeneously dispersed in the cages of zeolite Y. Since the encapsulation of Si clusters takes place within the α-cages and each unit cell of zeolite Y contains eight α-cages, the individual Si cluster appears on average to contain about 9−10 unoxidized Si atoms, which account for the bulk of the Si cluster. From the Si K-edge XANES edge jump for SiO_x species, which we assume bridge the cluster to the zeolite framework, we can also estimate that there are roughly two to three partly oxidized Si atoms per cluster. The total number of Si atoms in the cluster must therefore be ~12 with an estimated error of ±2. Taking into consideration the fact that a certain amount of Si is lost as SiH_4 during thermolysis, this Si cluster size determined by XPS/XANES is quite consistent with the number of entrapped disilane precursors measured by ^{1}H NMR spin counting.

The space of the 13-Å α-cage could, in theory, accommodate clusters of Si with a diamond-like lattice structure of perhaps over 60 Si atoms,[13b] far more than are observed. However, the volume of the cage is only ~10 times the volume of the disilane molecule, and this does not take into account the dead space that must be left when the molecules are packed into the cage. This, combined with mass transport difficulties, especially at

(40) (a) Schuppler, S.; Friedman, S. L.; Marcus, M. A.; Adler, D. L.; Xie, Y. H.; Ross, F. M.; Chabal, Y. J.; Harris, T. D.; Brus, L. E.; Brown, W. L.; Chaban, E. E.; Szajoski, P. F.; Christman, S. B.; Citrin, P. H. *Phys. Rev. B* **1995**, *52*, 4910. (b) Lee, P. A.; Citrin, P. H.; Eisenberger, P.; Kincaid, B. M. *Rev. Mod. Phys.* **1981,** *53*, 769.

(41) Stohr, J. *NEXAFS Spectroscopy*; Springer-Verlag: Berlin, 1992.

(42) Kasrai, M.; Lennard, W. N.; Brunner, R. W.; Bancroft, G. M.; Bardwell, J. A.; Tan, K. H. *Appl. Surf. Sci.* **1996**, *99*, 303.

high disilane loadings, conspires to keep the maximum size of the cluster to the relatively small values observed. In other words, the vehicle used to get the Si atoms into the cage itself restricts the number admitted. Similar observations of restricted cluster size have also been found in Ge[10] and II−VI[8b] semiconductor clusters.

Band Gap. In this part of the work, we used X-ray absorption and photoemission spectroscopies to measure the energies of the conduction (LUMO) and valence (HOMO) band edges of the Si cluster. Changes in the microstructure of Si may result in changes of electronic states and, thus, band edge energies. From the energy shifts of the band edges relative to those of c-Si, one should be able to obtain the HOMO−LUMO band gap of the cluster, a key aspect of the cluster's electronic structure. Such electronic information can give insight into the understanding of the photoluminescent properties of the Si clusters. A combination of X-ray absorption and photoemission spectroscopies has been used recently to measure the band gap in porous silicon.[43]

The inset in Figure 9 shows the comparisons of Si K-edge absorption for c-Si and the intrazeolitic Si cluster. Both Si K-edge absorption spectra were calibrated to the position of the SiO_2 peak at 1847.24 eV, so that any energy-level shifts caused by charging effects and/or induced by surface Fermi-level changes can be eliminated. The onset of absorption edge is measured by a linear extrapolation of the low absorption energy edge of each sample. It can be seen that the absorption edge for the Si cluster is blue-shifted ~0.4 eV relative to that of c-Si.; i.e., the LUMO energy level in the Si cluster is 0.4 eV higher than the conduction band minimum in c-Si. A blueshift of 0.4 eV in Si L-edge absorption has also been observed in the Si clusters relative to c-Si.[19] Similar observations in Si K-edge absorption were also reported on other nanostructured Si systems, e.g., porous Si[44] and layered polysilane.[45]

Figure 10a shows the valence band spectra for $H_{32}Na_{24}Y$ with and without the Si clusters. Because zeolitic materials are nonconductive, the photoemission current creates a positive charge in the sample which also shifts the photoemission spectrum to higher binding energy and broadens the signals. The magnitude of this shifting is about the same in both samples. Therefore, subtracting these two spectra should produce the valence band of Si_n clusters. To compare the valence band edge of the clusters with that of c-Si, we calibrated the respective spectra with the Si 2p core level following the reported procedure.[43] The corrected valence band spectrum for the Si_n cluster is compared with that of c-Si in Figure 10b. As with the Si K-edge absorption, the onset of the valence band edge is also obtained by a linear extrapolation of the low binding energy edge of the photoemission spectrum. Clearly, the valence band edge in Si_n clusters has a 0.7 eV higher binding energy than c-Si, which puts the HOMO energy level in Si_n clusters 0.7 eV lower than the valence band maximum in c-Si. It is noteworthy that the shift of HOMO energy level is significantly larger than that of the LUMO energy level. This trend is consistent with recent experimental studies on porous Si[41] and the calculations on hydrogenated Si clusters.[46]

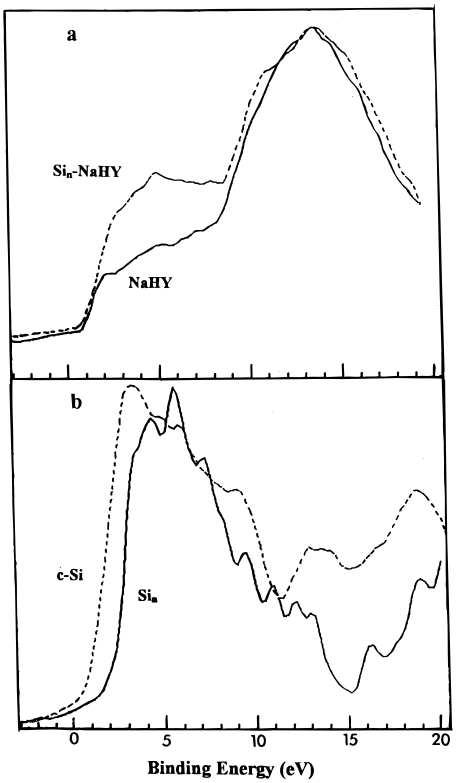

Figure 10. Valence band spectra for (a) $H_{32}Na_{24}Y$ and Si clusters/$H_{32}Na_{24}Y$ and (b) c-Si and Si clusters (the latter obtained by subtraction: Si clusters/$H_{32}Na_{24}Y$ minus $H_{32}Na_{24}Y$).

Taking together the sum of the HOMO and LUMO band edge shifts and the indirect band gap of c-Si (1.1 eV),[47] the band gap (HOMO−LUMO) of the Si clusters is ~2.2 eV. This result agrees very well with the photoluminescence (PL) peak energy (2.2 eV, see below) and the optical gap (2.22 eV) on similar Si_n clusters in zeolite HY reported by Ozin's group.[11a] This value is much smaller than the 3−4-eV band gap calculated theoretically for "free" Si clusters of similar size.[48] However, since the intrazeolitic Si clusters are capped by both oxygen and hydrogen, a direct comparison with "free" Si clusters may not be appropriate. Furthermore, it has been pointed out from theory that the orbital hybridization and the bonding in small clusters are very sensitive to the size and shape of the clusters,[49] and there is a strong suggestion based on other experimental studies that the relationship between band gap and cluster size is not simple when the clusters are small.[50]

Photoluminescence. Prior to measuring the photoluminescence of intrazeolitic Si_n clusters, the luminescent behavior of the pristine $H_{32}Na_{24}Y$ host was evaluated. Only a weak emission was observed around 500 nm at room temperature. This may be associated with the hydroxyl groups. Figure 11 shows the room-temperature PL spectrum for the intrazeolitic Si_n clusters. The luminescence peak energy is ~560 nm (2.2 eV), which is the same as its HOMO−LUMO band gap. The PL peak is very close to the luminescence at 2.25 eV from *syn*-tricyclooctasilane.[51] This similarity leads us to propose that the Si clusters may have a ladderlike structure as in *syn*-tricycloo-

(43) van Buuren, T.; Tiedje, T.; Dahn, J. R.; Way, B. M. *Appl. Phys. Lett.* **1993**, *63*, 2911.
(44) (a) van Buuren, T.; Gao, Y.; Tiedjie, T.; Dahn, J. R.; Way, B. M. *Appl. Phys. Lett*. **1992**, *60*, 3013. (b) Dahn, J. R.; Way, B. M.; Fuller, E. W.; Weydanz, W. J.; Tse, J. S.; Klug, D. D.; Van Buuren, T.; Tiedje, T. *J. Appl. Phys*. **1994**, *75*, 1946.
(45) He, J.; Tse, J. S.; Klug, D. D.; Preston, K. *J. Mater. Chem*. **1998**, *8*, 705−710.
(46) Ren, S. Y.; Dow, J. D. *Phys. Rev. B* **1992**, *45*, 6492.
(47) Bludau, W.; Onton, A.; Heiker, W. *J. Appl. Phys*. **1974**, *45*, 1974.
(48) (a) Wang, L.-W.; Zunger, A. *J. Chem. Phys.* **1994**, *100*, 2394. (b) Delerue, C.; Allan, G.; Lannoo, M. *Phys. Rev. B* **1993**, *48*, 11024.
(49) (a) Raghavachari, K.; Logovinsky, V. *Phys. Rev. Lett*. **1985**, *55*, 2853. (b) Raghavachari, K.; Rohlfing, C. M. *J. Chem. Phys*. **1988**, *89*, 2219.
(50) Kanemitsu, Y.; Suzuki, K.; Kondo, M.; Kyushin, S.; Matsumoto, H. *Phys. Rev. B* **1995**, *51*, 10666.

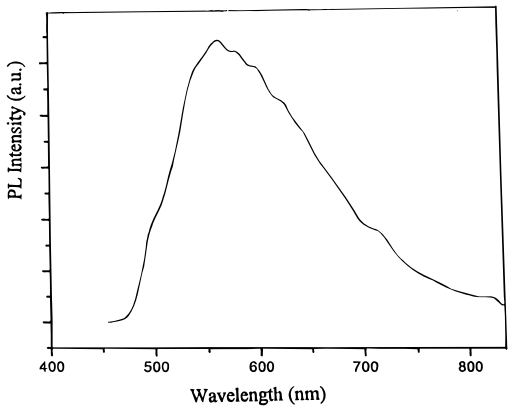

Figure 11. Room-temperature photoluminescence spectrum for the Si clusters/$H_{32}Na_{24}Y$ sample (with 488-nm Ar^+ laser excitation).

tasilane. These results also further confirm that the luminescence indeed originates from the encapsulated Si clusters and not from other sources such as hydroxyl groups in the zeolite. The consistency between the luminescence peak and the band gap suggests that the luminescence arises predominantly from a radiative electron−hole recombination between the HOMO and LUMO levels, and no midgap surface states or defects are involved.

Samples with Si cluster sizes lower than the saturated Si loading also display strong room-temperature photoluminescence in the same region. The PL intensity increases with the number of Si per unit cell; however, its peak energy does not appear to shift appreciably. This observation indicates that discrete Si clusters are formed only inside the cages and that they become more homogeneously dispersed in the zeolite host with increase of Si loading.

Conclusion

In the continuing quest for nanoscale clusters of silicon with interesting optical and electronic properties, we have succeeded in obtaining a coherent picture of the nature of Si clusters encapsulated in the large cages of Y zeolite. The clusters were produced by adsorbing and anchoring disilane at the acid and ion sites in the large cage of NaHY zeolite, followed by thermolysis to produce clustering. Steric restrictions imposed by the host ensure that disilane molecules are exclusively entrapped in the α-cage.

The difficult task of characterizing the clusters required the application of both conventional and unconventional techniques: (a) Infrared spectroscopy and ^{29}Si CP MAS NMR showed the anchoring of $-Si_2H_5$ groups at Brønsted acid sites on the zeolite cage walls, plus additional adsorption of Si_2H_6. (b) ^1H NMR multiple-quantum spin counting showed that the saturation loading of disilane molecules in the cage at the precursor stage is 7. Thus, the average number of silicons in the final cluster can be no more than 14 Si. (c) Mass spectrometry showed that some Si is lost as SiH_4 during thermolysis, so the average cluster size must be less than 14 Si. (d) XPS and Si K-edge XANES results showed a maximum average cluster size of 12 Si atoms/cage, with some of the Si atoms still attached to O atoms in the zeolite framework. (e) ^1H NMR spin counting also showed that the clusters contain four to five H atoms.

The cluster therefore consists of 12 Si atoms, terminated by H atoms and by O atom connections to the zeolite framework. One possible model is a ladderlike configuration of linked Si atoms with the top and bottom attached to the zeolite and the end of each rung capped by an H atom.

Synchrotron photoabsorption and photoemission spectra gave a determination of the HOMO−LUMO band gap of this material of 2.2 eV, very similar to the peak energy of the photoluminescence spectrum. This suggests that the photoluminescence arises from an electron−hole recombination process.

Acknowledgment. We thank Mr. Regent Dutrisac for technical assistance in sample preparation, Mr. Gerald Pleizier for recording the XPS data, and Dr. C. Bowes for valuable discussion.

JA9816133

(51) (a) Kanemitsu, Y.; Suzuki, K.; Uto, H.; Masumoto, Y.; Matsumoto, T.; Kyushin, S.; Higuchi, K.; Matsumoto, H. *Appl. Phys. Lett.* **1992**, *61*, 2446. (b) Kyushin, S.; Matsumoto, H.; Kanemitsu, Y.; Goto, M. *J. Phys. Soc. Jpn.* **1994**, *63*, 46.